NiWO$_4$-ZnO-NRGO ternary nanocomposite as an efficient photocatalyst for degradation of methylene blue and reduction of 4-nitro phenol

M. Mohamed Jaffer Sadiq [a], U. Sandhya Shenoy [b], D. Krishna Bhat [a, *]

[a] Department of Chemistry, National Institute of Technology Karnataka, Surathkal, Mangalore 575025, India
[b] Jawaharlal Nehru Centre for Advanced Scientific Research, Jakkur, Bangalore 560064, India

A B S T R A C T

A novel NiWO$_4$-ZnO-NRGO ternary nanocomposite has been efficiently synthesized by decorating nitrogen doped reduced graphene oxide (NRGO) with zinc oxide and nickel tungstate nanoparticles via a facile microwave irradiation technique and its capability to catalyze photodegradation of methylene blue (MB) dye in aqueous solution and reduction of 4-nitro phenol (4-NP) to 4-amino phenol (4-AP) using sodium borohydride was explored. The as-synthesized nanocomposite was characterized by X-ray diffraction (XRD), Raman spectroscopy, Brunauer-Emmett-Teller (BET) analysis, energy dispersive X-ray (EDX) analysis, field emission scanning electron microscopy (FESEM), transmission electron microscopy (TEM), high-resolution transmission electron microscopy (HRTEM), X-ray photoelectron spectroscopy (XPS), photoluminescence (PL) spectroscopy and diffuse reflectance spectroscopy (DRS) techniques. The photocatalytic activity of the as-synthesized nanocomposite estimated through the photodegradation of MB under visible light irradiation showed 9 times improvement over pure NiWO$_4$. It also showed excellent catalytic activity in reduction of 4-NP to 4-AP. The material also showed excellent stability and reusability. The entire study revealed that the novel NiWO$_4$-ZnO-NRGO ternary nanocomposite can act as a promising bifunctional photocatalyst for environmental remediation and industrial application.

1. Introduction

In last few decades, water pollution due to industrial effluents has become a huge concern for the environment [1]. Waste water released from various industries containing toxic chemicals has posed a threat to aquatic as well as human life. In such a situation development of new strategies for environmental remediation is the need of the day. Photocatalysis has emerged as a savior in this respect. Nanoparticles like ZnO, NiO, TiO$_2$, Fe$_3$O$_4$, Co$_3$O$_4$ and their composites show a great promise as photocatalysts due to their excellent physical and chemical properties [2–6]. Likewise, metal tungstates have also attracted attention due to their band gap tunability when coupled with other semiconductors [7–10]. Reduced graphene oxide (RGO) is a single-atom thick sheet formed by sp^2-bonded carbon atoms packed into a 2D hexagonal lattice. It has desirable properties like large surface area; better chemical and mechanical strength; good optical, electrical and thermal properties [11,12].

In order to achieve excellent catalytic performance in nanocomposites two important factors have to be considered: faster electron transfer and better charge separation. A combination of semiconductors with suitable band gaps can promote charge carrier separation [13]. There are many reports on the incorporation of carbon nanostructures such as graphene and carbon nanotubes as components of photocatalyst composites to enhance the activity [14–19]. The incorporation of nitrogen atoms which are rich in electrons, into RGO promotes the interaction between neighboring carbons atoms and electrons. NRGO increases the transfer rate of electron from the conduction band (CB) of the semiconductor and also creates an additional donor level above the valence band of semiconductors thereby reducing the energy requirement for the excitation of electron from valance band (VB) to CB of semiconductor materials [20,21]. The ternary composites have better charge carrier separation and a fast electron transfer system compared to the pristine semiconductor materials [22]. However, excellent catalytic performance with high stability and low cost are still rare [23].

In view of the aforementioned facts a novel NiWO$_4$-ZnO-NRGO ternary nanocomposite has been efficiently synthesized via a facile, cost effective microwave irradiation technique. The as-synthesized nanocomposite was characterized by diffraction, microscopic, spectroscopic

---

* Corresponding author.
  E-mail address: denthajekb@gmail.com (D.K. Bhat).

techniques to study the elemental composition, morphology and optical properties. The photocatalytic efficiency was studied in photodegradation of MB dye in aqueous solution and hydrogenation of 4-NP to 4-AP using sodium borohydride. The ternary composite shows excellent photocatalytic activity, stability and reusability compared to the pristine materials. This bifunctional photocatalyst shows a huge promise in environmental remediation and industrial application. To the best of our knowledge this is the first report on synthesis and study of photocatalytic activity of NiWO$_4$-ZnO-NRGO ternary composite in degradation of MB and hydrogenation of 4-NP.

2. Experimental

2.1. Materials and method

All the reagents and chemicals were obtained from Sigma-Aldrich and were utilized without additional purification. Millipore water was used to carry out all the experiments.

2.2. Preparation of NiWO$_4$ and ZnO nanomaterials

To synthesize NiWO$_4$, 0.01 M of nickel acetate solution and 0.01 M of sodium tungstate solution were stirred for 1 h. The mixture was irradiated with microwave for 10 min at 350 W. The obtained precipitate was cooled, centrifuged and washed with water and ethanol. It was finally dried at 80 °C for 12 h. For synthesis of ZnO the same procedure was employed, but by using zinc acetate and sodium hydroxide solution in 1:2 ratio.

2.3. Preparation of the ternary NiWO$_4$-ZnO-NRGO ternary nanocomposites

GO was prepared by modified Hummers method as reported elsewhere [24,25]. NiWO$_4$-(A)-ZnO-(B)-NRGO ternary nanocomposites (A = 0, 0.005, 0.01 and 0.02 M of zinc precursor solution; B = 0.5, 1, 2.5 and 5 wt. % GO) were synthesized via microwave irradiation method. In a typical synthesis, 0.01 M of nickel acetate solution and 0.01 M of sodium tungstate solution was slowly added to the dispersed GO solution under consistent stirring for approximately 2 h. During this calculated amount of zinc acetate and sodium hydroxide was also added. The pH of the solution was maintained at 9 using ammonia. Later, 1% urea was added to the above mixture. The resulting solution was irradiated with microwave (350 W) for 10 min and the obtained precipitate was allowed to cool naturally. The precipitate was centrifuged and washed several times with water and ethanol and then finally dried at 80 °C for 12 h. Control samples containing RGO was synthesized in the absence of urea.

2.4. Characterization

The phase structure and purity of the nanocomposites were investigated using XRD (Rigaku) with Cu-K$_\alpha$ radiation for 2θ range of 5°–70° with a scan rate of 1°/minute. Raman spectrum was recorded at 532 nm using the laser Raman microscope (Renishaw, Invia) equipped with He-Ne laser source. Nitrogen adsorption and desorption experiments were performed at 77 K on a Micromeritics ASAP 2020 system. Prior to analysis, the samples were degassed at 200 °C in vacuum for 24 h. The specific surface area (SSA) was calculated by the Brunauer-Emmett-Teller (BET) method based on adsorption data in the relative pressure (P/Pº) range of 0.05–0.3. The pore size distribution was calculated using the Barrett-Joyner-Halenda (BJH) model applied to the desorption branch. The morphology of the samples was studied using field emission scanning electron microscope (FESEM, Zeiss Ultra 55), transmission electron microscope (TEM, Tecnai G20) and high-resolution transmission electron microscope (HRTEM, Tecnai). Elemental composition was determined using EDX (Zeiss Ultra 55) and XPS (Kratos XSAM800) equipped with a standard monochromatic Al K$_\alpha$ source. UV–visible spectrum was

obtained by diffuse reflectance method (Analytic Jena). The photoluminescence (PL) spectrum was recorded using fluorescence spectrophotometer (Horiba JobinYvon). The total organic carbon concentration (TOC) was measured using total organic carbon analyzer (TOC-V CSN, Shimadzu, Japan).

2.5. Determination of photocatalytic activity

Photocatalytic properties of the ternary nanocomposites were studied using MB following procedure reported elsewhere [22]. 20 mg of nanocomposites were dispersed in 200 mL aqueous solution of 10 mg/L MB dye and stirred for 30 min in the dark to attain adsorption desorption equilibrium. Later, this solution was exposed to a 250 W Hg lamp provided with a cutoff filter of 400 nm. At regular time intervals, 4 mL of the MB solution was withdrawn and centrifuged to remove the residual nanocomposites. The supernatant was used to record the absorbance at 664 nm wavelength. The percentage of photodegradation of the MB dye was calculated using equation (1).

$$\text{Percentage of photodegradation of the MB dye} = \left[(C_o - C)/C_o \right] \times 100 \quad (1)$$

where, C_o is the initial concentration and C is the concentration at a given interval time, of the MB dye solution, respectively.

To determine the possible photocatalytic degradation mechanism, trapping experiments were conducted using various kinds of scavengers. In trapping experiments, the photocatalytic activity of the catalyst was determined under similar conditions as outlined above in the presence of a scavenger for a particular species.

The mineralization of the dye was calculated by using TOC analysis. The TOC was analyzed before the start of the experiment (TOC$_o$) and at specified intervals during the photodegradation reaction (TOC$_t$). The % mineralization of MB dye was calculated by using the following equation (2).

$$\% \text{ Mineralization of the MB dye} = \left[(TOC_o - TOC_t)/TOC_o \right] \times 100 \quad (2)$$

where, TOC$_o$ is the initial concentration and TOC$_t$ is the concentration at a given interval time, of the MB dye solution, respectively.

2.6. Reduction studies

In a typical experiment, 2.7 mL of 4-NP (0.1 mM) was mixed with 0.3 mL of NaBH$_4$ (0.1 M) solution under constant magnetic stirring followed by addition of 0.1 mg of catalyst. The reduction reaction of 4-NP was investigated using UV–visible absorption spectroscopy in the range of 250 nm–500 nm. Once the reaction completed the recovery of the catalyst was done by ultracentrifugation, followed by thorough washing with 10% ethanol and finally vacuum drying at 60 °C for 6 h. The catalyst was then reused for subsequent cycles to study its stability and reusability.

3. Results and discussion

3.1. XRD studies

Fig. 1 reveals the XRD patterns of the as-synthesized GO, NiWO$_4$, ZnO and NiWO$_4$-0.01 M ZnO-2.5% NRGO. The diffraction peaks at 10.5° corresponds to (002) planes of GO sheets. ZnO diffraction peaks at 31.6°, 34.2°, 36.1°, 47.4°, 56.4°, 62.7°, 66.2°, 67.8° and 68.9° can be indexed to the (100), (002), (101), (102), (110), (103), (200), (112) and (201) as indicated in JCPDS file no. 36-1451 [26]. NiWO$_4$ diffraction peaks at 19.2°, 24.1°, 24.8°, 30.9°, 31.5°, 36.7°, 38.7°, 41.6°, 44.9°, 49.1°, 50.6°, 52.0°, 54.2°, 65.2° and 68.6° is ascribed to the (100), (011), (110), (111), (020), (002), (200), (102), (112), (022), (220), (130), (202), (132) and (041) planes according to JCPDS file no. 15-0755. Peaks corresponding to NRGO were not found in the diffraction pattern of ternary composite.
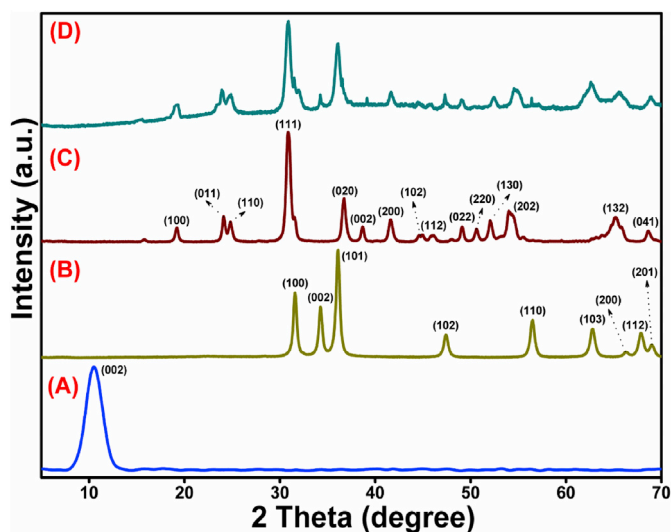
Fig. 1. XRD spectrum of (A) GO, (B) NiWO$_4$, (C) ZnO and (D) NiWO$_4$-0.01 M ZnO-2.5% NRGO.
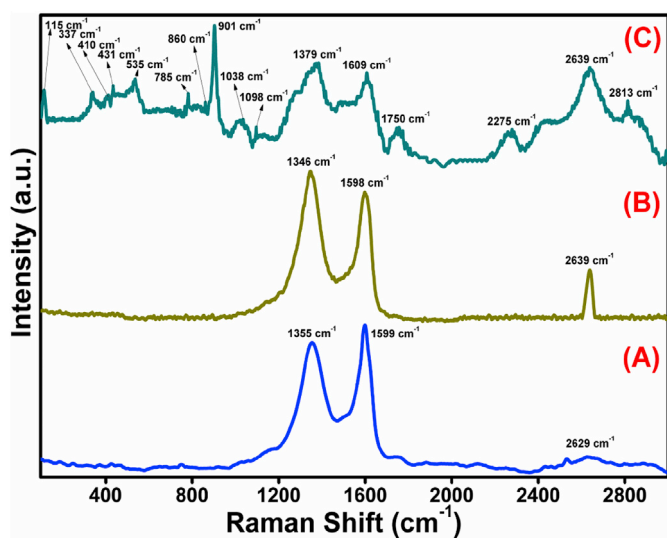

Fig. 2. Raman spectra of (A) GO, (B) NRGO and (C) NiWO$_4$-0.01 M ZnO-2.5% NRGO.

This may be due to the small quantity and exfoliated nature of NRGO in the composite [21].

3.2. Raman studies

Raman spectrum of GO (Fig. 2A) reveals two distinct modes: G mode at 1599 cm^{-1} and D mode at 1355 cm^{-1}. The intensity ratios of D to G band (I_D/I_G) is a measure of relative concentration of sp^3 hybridized defects to sp^2 hybridized GO domains [27]. We see that after microwave irradiation the I_D/I_G ratio increases from 0.87 for GO to 1.09 for the composite indicating the formation of more defects in NRGO (Fig. 2B) during the reduction. Slight variation in the Raman frequency, appearance of a prominent 2D band at 2639 cm^{-1} in Fig. 2B may be attributed to the formation of NRGO from GO.

Fig. 2C shows the Raman spectrum of NiWO$_4$-0.01 M ZnO-2.5% NRGO ternary nanocomposite. Raman bands at 785 cm^{-1}, 901 cm^{-1} and 1038 cm^{-1} correspond to Raman active modes of NiWO$_4$. Bands at 115 cm^{-1}, 337 cm^{-1}, 410 cm^{-1}, 431 cm^{-1}, 535 cm^{-1}, 860 cm^{-1}, 1098 cm^{-1}, 1750 cm^{-1}, 2275 cm^{-1} and 2813 cm^{-1} correspond to the Raman active modes of ZnO. Peaks at 1379 cm^{-1} (D mode);

1609 cm^{-1} (G mode) with I_D/I_G ratio 1.10 and 2D band at 2639 cm^{-1} with I_{2D}/I_G ratio as 1.06 correspond to presence of double layered NRGO with defects in the ternary composite. The change in the value of Raman frequencies of D and G band and increased value of I_D/I_G ratio in the composite may be due to the interaction between the NRGO sheets and the semiconductor particles [21].

3.3. BET surface area analysis

The nitrogen adsorption-desorption isotherms were used to obtain information about the BET specific surface area and pore size distribution in the nanocomposites [28]. As observed in Fig. 3, the isotherm exhibits a characteristic type-IV pattern with a significant hysteresis in the P/P$_o$ range 0.6–1.0, implying the existence of abundant mesopores in the synthesized nanocomposites. The slightly wide capillary condensation step is a consequence of the relatively broad pore size distribution, as shown in Fig. 3.

BET analysis showed that the specific surface area of NiWO$_4$, NiWO$_4$-2.5% NRGO and NiWO$_4$-0.01 M ZnO-2.5% NRGO are 25.25 m^2/g, 34.64 m^2/g and 38.83 m^2/g, respectively. From these results, it is evident that the higher surface area of NiWO$_4$-2.5% NRGO and NiWO$_4$-0.01 M ZnO-2.5% NRGO nanocomposites than that of pure NiWO$_4$, is due to the contribution from NRGO and ZnO components. The pore size distribution calculated by the BJH method indicates that the nanocomposite has a hierarchical pore structure, the sizes of which peak at 3.34 nm and 5.61 nm. The presence of such mesopores is believed to increase the total surface area which in turn would enhance the catalytic activity of the ternary nanocomposites.

3.4. Morphology studies

The morphology of the samples was studied using electron microscopy. The FESEM images of the NiWO$_4$ and ZnO (Figs. S1A–B) suggest that the particles have approximately spherical shape. Similarly (Fig. 4A) reveals that the NiWO$_4$-0.01 M ZnO-2.5% NRGO ternary nanocomposite consists of ZnO and NiWO$_4$ nanoparticles well anchored on the surface of the NRGO sheets. This observation is further supported by the TEM image (Fig. 4B). EDX spectra of the encircled areas are shown in Fig. 4C–D. HRTEM image in Fig. 5A shows the interface between NiWO$_4$, ZnO and NRGO in NiWO$_4$-0.01 M ZnO-2.5% NRGO ternary nanocomposite. The obtained lattice fringes of 0.15 nm correspond to the (111) plane of NiWO$_4$ and that of 0.283 nm correspond to the (100) plane of ZnO. The EDX spectrum (Fig. 5B) revealed N, C, O, Ni, Zn and W as the elements present in the composite. Uniform distribution of the particles is indicated by elemental mapping (Fig. 5C–H). The average size of the nanoparticles was found to be 13.4 nm for NiWO$_4$ and 22.7 nm for ZnO (Fig. S2).

3.5. XPS studies

The XPS survey spectrum of NiWO$_4$-0.01 M ZnO-2.5% NRGO nanocomposites is shown in Fig. S3 and detailed elemental compositions are summarized in Table S1. The binding energy positions in the XPS spectrum were calibrated with C *1s* at 284.8 eV. Fig. 6A shows the C *1s* spectra which can be deconvoluted into five peaks at 284.5 eV (CC/CC), 285.5 eV (CN), 286.1 eV (CO), 287.2 eV (CO) and 290.2 eV (OCO), respectively [22]. Fig. 6B reveals the N *1s* spectra which can be deconvoluted into four peaks at 398.4 eV (pyridinic-N), 399.4 eV (pyrrolic-N), 400.8 eV (graphitic-N) and 402.4 eV (pyridine-*N*-oxide), respectively [21]. Fig. 6C depicts Ni *2p* spectra deconvoluted into six peaks located at 855.9 eV, 857.7 eV (satellite), 861.6 eV which belongs to Ni *2p$_{3/2}$* and 873.6 eV, 875.4 eV (satellite), 879.5 eV which belongs to the Ni 2p$_{1/2}$, respectively [29]. Fig. 6D shows the W *4f* spectra deconvoluted into four peaks corresponding to W *4f$_{7/2}$* (34.8 eV and its satellite 35.4 eV) and W *4f$_{5/2}$* (36.9 eV and its satellite 37.5 eV), respectively [24]. Fig. 6E shows the Zn *2p* spectra deconvoluted into four peaks placed at 1018.1 eV,
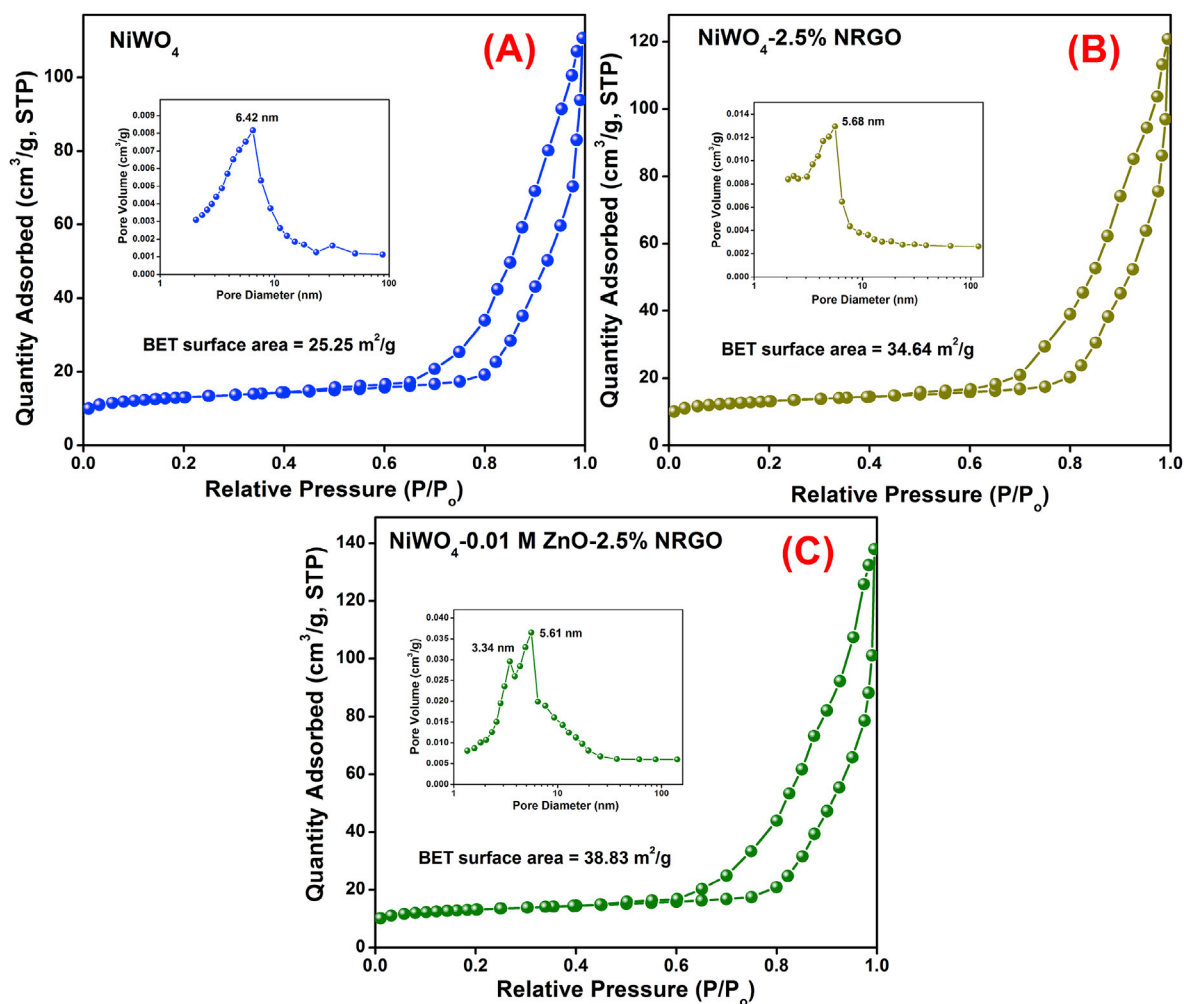
Fig. 3. BET surface area analysis: Adsorption-desorption isotherms.

1019.6 eV (satellite) which belongs to Zn $2p_{3/2}$ and 1041.1 eV, 1042.5 eV (satellite) belongs to the Zn $2p_{1/2}$, respectively [24]. Fig. 4F reveals O *1s* spectra deconvoluted into three peaks at 530.2 eV, 532.2 eV and 533.1 eV related to ZnO, $NiWO_4$ and HOH bonds, respectively [21,22].

3.6. Optical absorbance analysis

The optical properties of the as-synthesized nanocomposites are studied by DRS. The absorption of ZnO-2.5% NRGO and $NiWO_4$-2.5% NRGO (Fig. 7) is high in comparison to pure ZnO and $NiWO_4$. The optical energy band gap (Fig. 7B) of the nanocomposites was measured using the Tauc relation, $\alpha h\nu = A (h\nu - E_g)^{n/2}$, where α, h, ν, E_g and n denote the absorption coefficient, Planck's constant, the velocity of light, energy band gap and the type of transition of the semiconductor. Among these parameters, 'n' is determined by the type of transition process that occurs in a semiconductor (n = 1 for a direct transition and n = 4 for an indirect transition). The direct band gap (i.e., n = 1) is considered in general for semiconductor photocatalysis processes [21,22]. The obtained band gap energy values of ZnO, $NiWO_4$, ZnO-2.5% NRGO, $NiWO_4$-2.5% NRGO and $NiWO_4$-0.01 M ZnO-2.5% NRGO are 3.0 eV, 3.10 eV, 2.82 eV, 2.42 eV and 2.27 eV, respectively. From the results, it is evident that there is an appreciable reduction in the band gap energy of the ternary nanocomposite in comparison with other components. This may be attributed to the synergic effect of the composite components, ZnO and NRGO leading to appreciable interaction among the components causing formation of new molecular orbitals of lower energy [21].

Using the DRS results, the band edge positions of the nanocomposites

were calculated theoretically using Mulliken electronegativity theory following the empirical equations (3) and (4).

$$E_{VB} = \chi - E^e + 0.5E_g \tag{3}$$

$$E_{CB} = E_{VB} - E_g \tag{4}$$

where E_{VB} is the valence band edge potential, E_{CB} is the conduction band edge potential, E_g is the band gap energy of the semiconductor, E^e is the scale factor of the hydrogen reference electrode (−4.5 eV), and χ is the absolute electronegativity of the semiconductor, which is defined as the geometric mean of the absolute electronegativities of the constituent atoms. The calculated band edge potentials of the CB and VB of ZnO and $NiWO_4$ are given in Table S2.

3.7. Photoluminescence analysis

An efficient photocatalyst should have very less recombination rate of photogenerated electron hole pair. The recombination of photogenerated electron-holes and charge separation in the ternary nanocomposite were investigated through PL emission spectrum as shown in Fig. S4. An intense PL peak corresponds to faster recombination rate of photo generated electron-hole pairs [22]. All the synthesized materials exhibited a broad emission peak in the visible region starting from 420 nm to 700 nm with the excitation wavelength of about 400 nm. Pure $NiWO_4$ showed an intense broad peak around 520 nm indicating rapid recombination of charge carriers. Introduction of NRGO led to slight
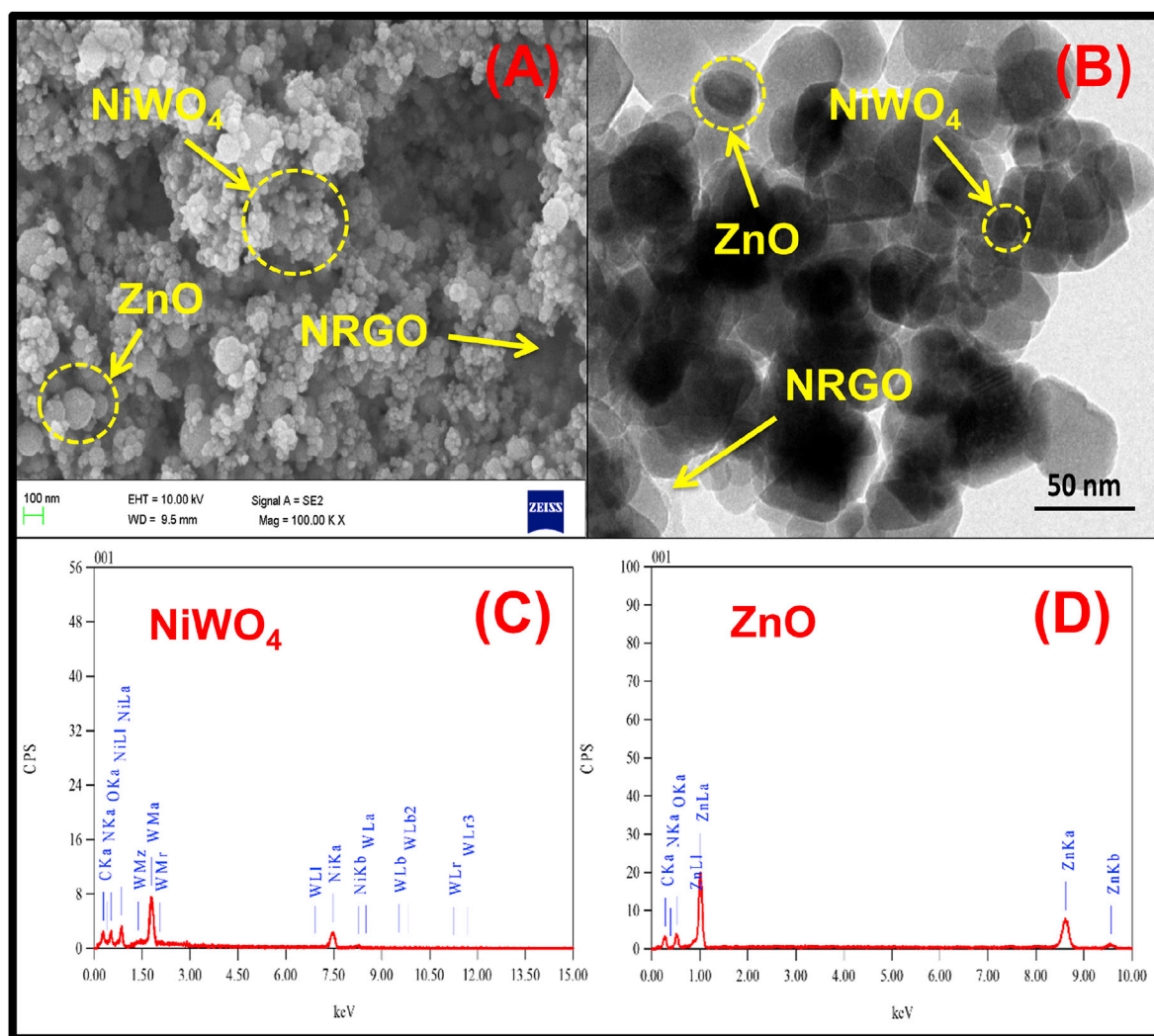
Fig. 4. (A) FESEM, (B) TEM image of NiWO$_4$ – 0.01 M ZnO – 2.5% NRGO ternary nanocomposite, EDX spectrum of (C) NiWO$_4$ and (D) ZnO nanoparticles present in the ternary composite.

decrease in PL intensity. The higher conductivity of the NRGO sheet matrix facilitates smooth electron transport and hence results in the increased separation of electron hole pairs [30]. Further, when ZnO is introduced, the PL spectrum of NiWO$_4$-0.01 M ZnO-2.5% NRGO nanocomposite exhibits very less intensity. This can be ascribed to the contribution of ZnO towards further separation of electron hole pairs. In the ternary composite, electrons are excited from VB to CB of ZnO and then immediately transported to the CB of NiWO$_4$ due to favorable energy level difference. From CB of NiWO$_4$ electrons would get transported through NRGO network due to the high conductivity of NRGO. Thus the entire process results in an efficient and enhanced separation of electron hole pairs and leads to appreciable decrease in the PL intensity in NiWO$_4$-0.01 M ZnO-2.5% NRGO nanocomposite [30–32].

3.8. Photocatalytic activity

The photocatalytic degradation of the as-synthesized nanocomposite was studied using MB solution under visible light irradiation. The blank test was performed without adding nanocomposite to MB solution. There was no noticeable degradation which indicated that the photolysis is insignificant for the blank MB solution. The NRGO composition in the nanocomposite was optimized based on the photodegradation efficiency. The photocatalytic efficiency of catalyst with varying NRGO content (Fig. S5) indicates that with increase in NRGO content the efficiency increases up to 2.5% NRGO and decreases there onwards. This decrease

in efficiency may be due to NRGO sheets covering the surface of semiconductor which in turn hinders the absorption of photon by the semiconductor. Such observations are well documented in the literature [9,10,17–19,22,25]. Hence NRGO content was kept constant at 2.5% and ZnO content was varied for further experiments.

The photocatalytic degradation efficiency with varied ZnO content (Fig. 8A) showed increase in efficiency with increase in ZnO content upto 0.01 M ZnO. NiWO$_4$-0.01 M ZnO-2.5% NRGO ternary composite showed maximum efficiency by degrading MB dye within 120 min. For sake of comparison even RGO composites were considered. RGO composites showed lesser efficiency than NRGO composites.

The as-prepared nanocomposite followed the first order kinetics of photocatalytic degradation of MB solution as given in equation (5)

$$\ln(C/C_o) = -kt \tag{5}$$

where, C_o is the initial concentration of the MB dye, C is the concentration of the MB at the irradiation time (t) and k is the first order rate constant. The rate constant k values were calculated from the slope of the straight line (Fig. 8B). Fig. 8C shows that the rate constant values of the different nanocomposites. The first order rate constants of ternary composite indicates 9 and 2.5 times more photocatalytic efficiency than the pure NiWO$_4$ and NiWO$_4$-2.5% NRGO, respectively.

The durability of the ternary nanocomposites was additionally investigated. It was seen that even after 5 consecutive cycles the
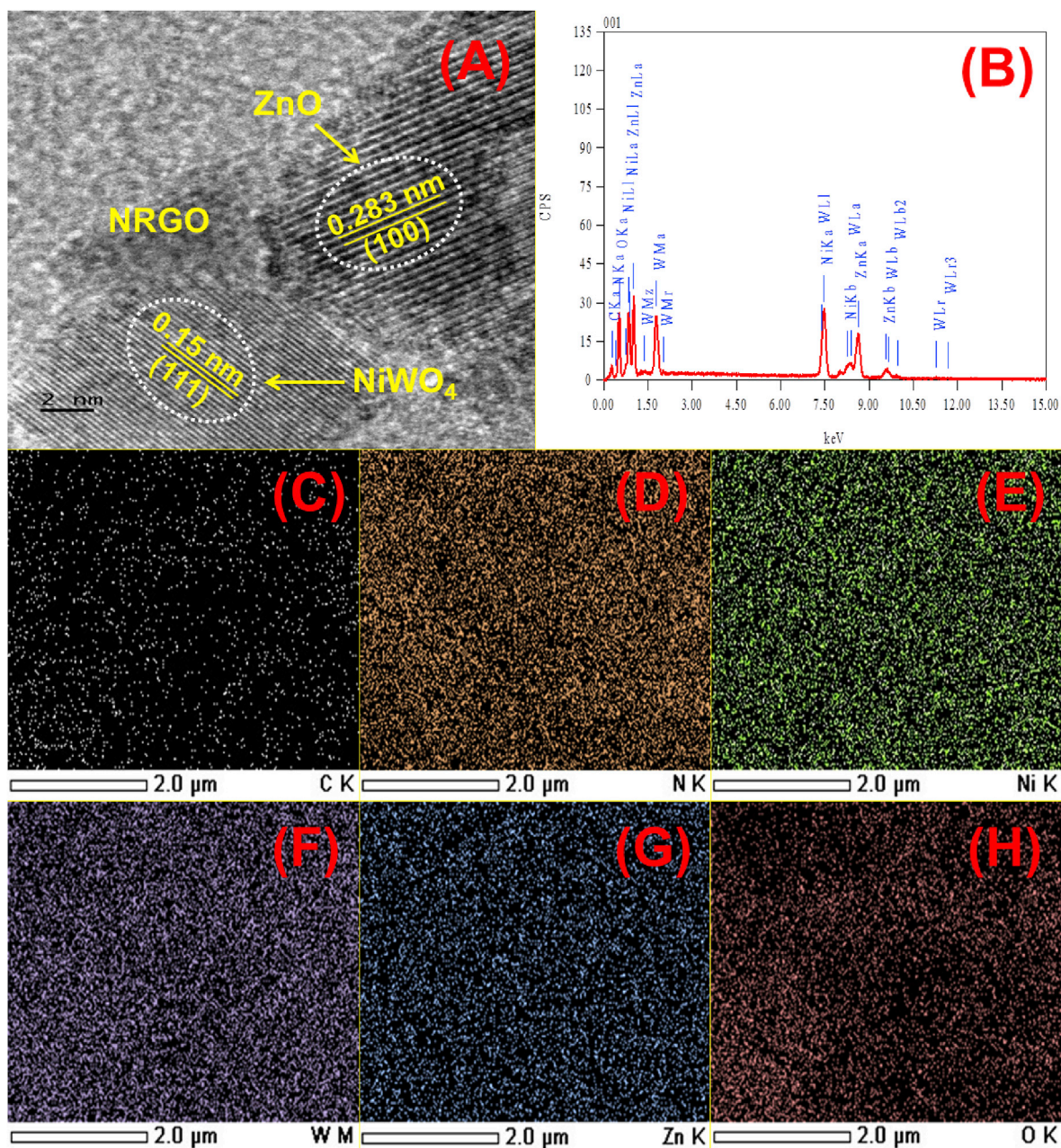
Fig. 5. (A) HRTEM image; (B) EDX spectrum; elemental mapping of (C) C; (D) N; (E) Ni; (F) W; (G) Zn and (H) O of $NiWO_4$ – 0.01 M ZnO – 2.5% NRGO ternary nanocomposite.

photocatalytic activity of nanocomposite showed only a small reduction in efficiency from 99.5% to 97.2%, which is negligible. The results indicate that the ternary composites have sufficient stability to be used in environmental applications.

To determine the degree of mineralization of MB, during its photodegradation catalyzed by $NiWO_4$-0.01 M ZnO-2.5% NRGO nanocomposite, total organic carbon (TOC) analysis was performed [33]. Fig. 9A shows the plot of absorbance vs. wavelength for MB at different time intervals. As can be observed from the plot, the absorbance at 664 nm decreased with time and reached 99.27% during scan at 120 min under visible light irradiation. Fig. 9B shows the TOC values for the MB solution at different intervals of time. The TOC value decreased to 88.28% under visible light irradiation for 120 min of visible light irradiation. Thus, it is very evident that, the $NiWO_4$-0.01 M ZnO-2.5% NRGO nanocomposite has high catalytic efficiency towards photodegradation of MB molecules and that organic carbon is mostly converted to CO_2 during the process.

Further, the recyclability of the ternary nanocomposite has also been investigated. It is observed that even after 5 consecutive cycles the efficiency of the photocatalytic activity of nanocomposite showed only a small reduction from 99.27% to 96.72%, which is negligible. The results therefore ascertain that the ternary composite also has sufficient stability for use in environmental applications.

3.9. Mechanism of the photocatalytic activity

To determine the active species involved in photodegradation and to find out the mechanism, trapping experiments were carried using scavenging agents such as, benzoquinone (BQ, a quencher of $O_2^{\bullet-}$), potassium iodide (KI, a quencher of h^+), silver nitrate ($AgNO_3$, a quencher of e^-) and ternary butanol (TBA, a quencher of OH•). Addition of TBA caused only a small decrease in efficiency (97.12%) which meant hydroxyl radical was not the active species. But addition of KI, $AgNO_3$ and BQ caused dramatic decrease in the efficiency 18.24%, 50.68% and 71.45%
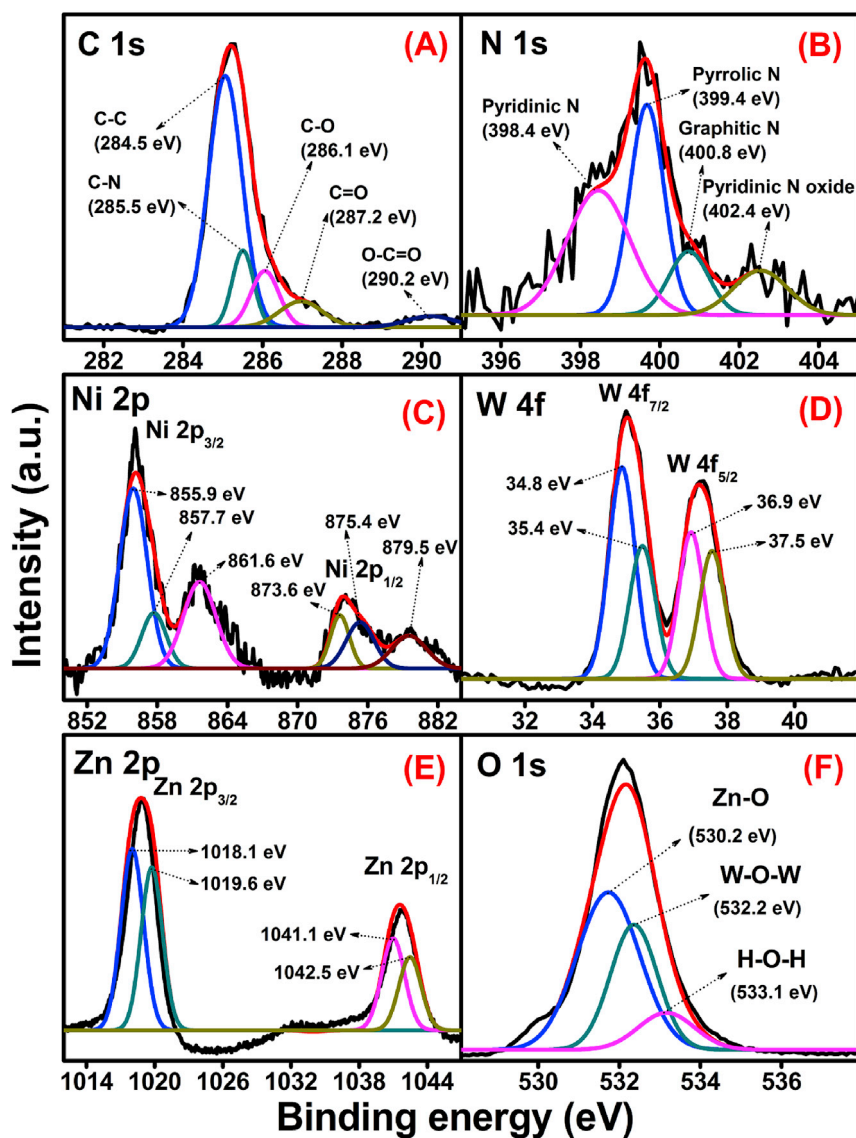
Fig. 6. High-resolution XPS spectra of NiWO$_4$-0.01 M ZnO-2.5% NRGO (A) C *1s*; (B) N *1s*; (C) Ni *2p*; (D) W *4f*; (E) Zn *2p* and (F) O *1s*.
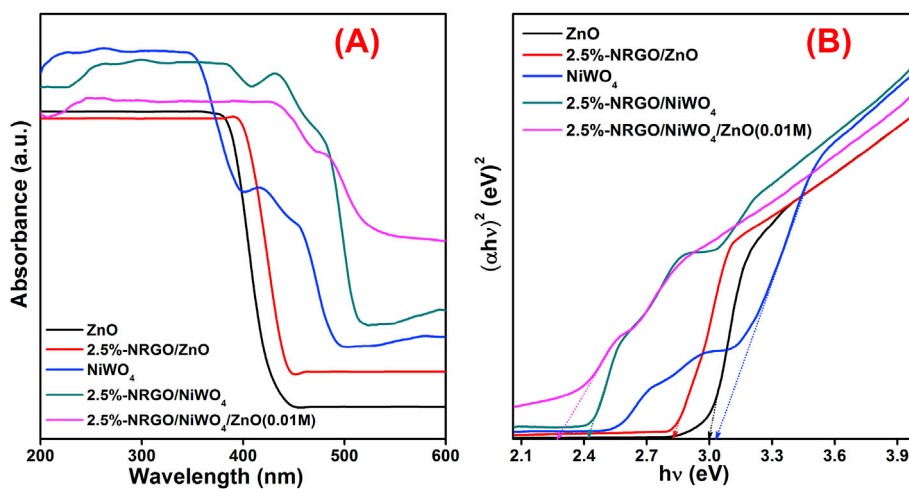

Fig. 7. (A) UV–Vis spectra and (B) band gap plots of ZnO, NiWO$_4$, ZnO-2.5% NRGO, NiWO$_4$-2.5% NRGO and NiWO$_4$-0.01 M ZnO-2.5% NRGO.
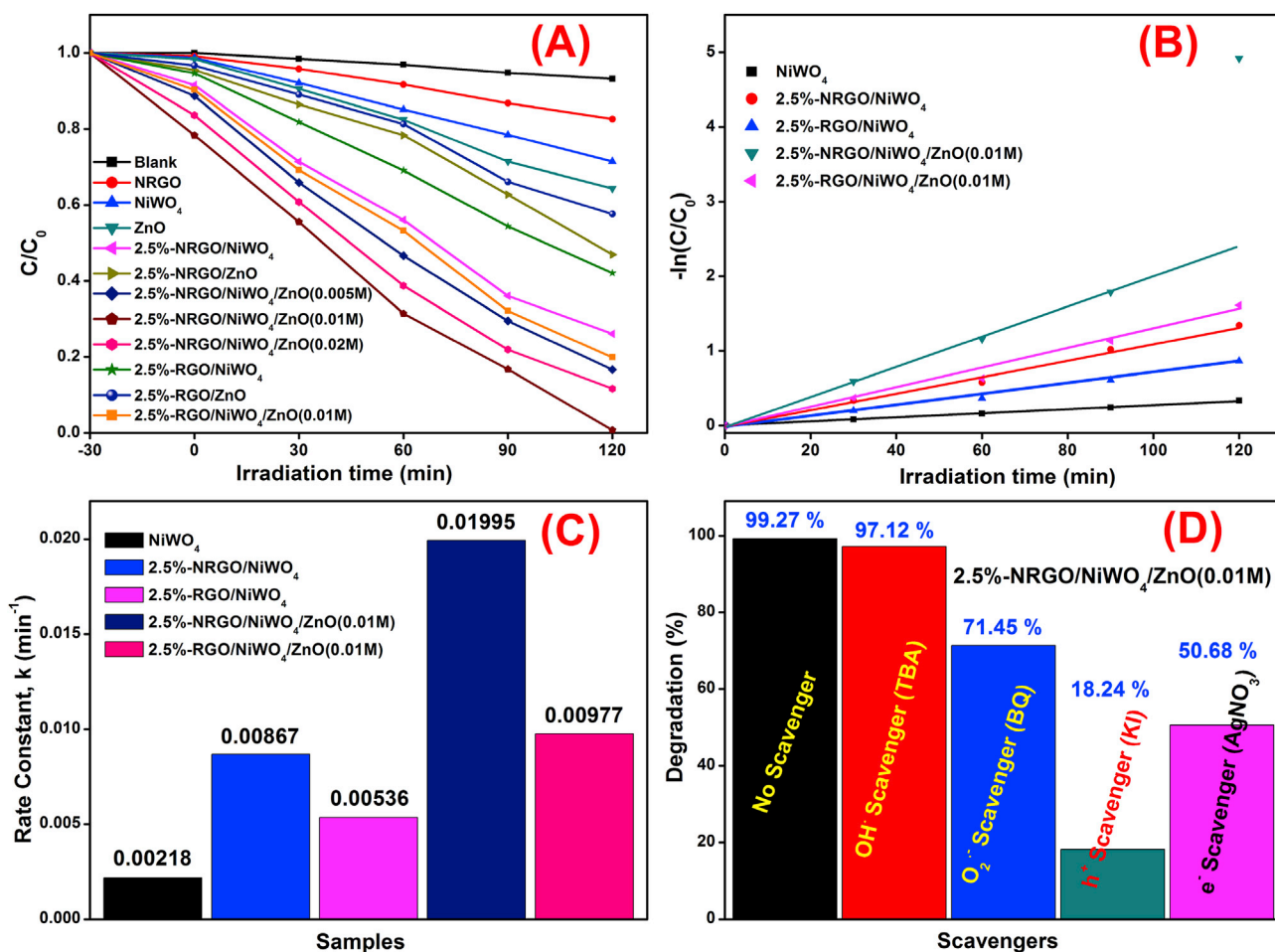
Fig. 8. (A) Degradation rate; (B) first order kinetics plot; (C) rate constants plot for the photodegradation of MB over various catalysts and (D) effects of different scavengers on the photodegradation of MB using $NiWO_4$-0.01 M ZnO-2.5% NRGO ternary composites under visible light irradiation.
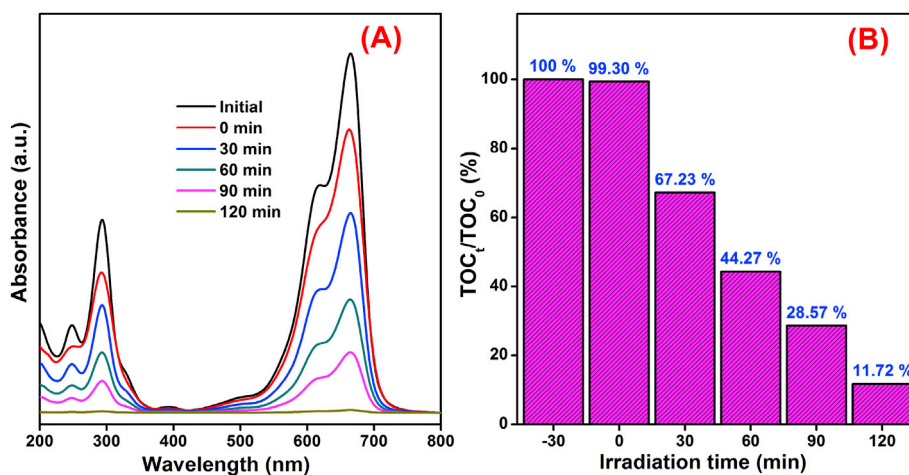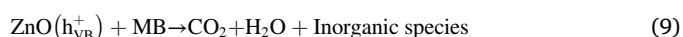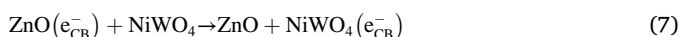

Fig. 9. (A) Absorbance versus wavelength and (b) TOC values for the MB solution at different intervals of time.

respectively. Based on these results the following mechanism is proposed.

$$ZnO + h\nu \rightarrow ZnO\left(e_{CB}^- + h_{VB}^+\right) \tag{6}$$

$$ZnO\left(e_{CB}^-\right) + NiWO_4 \rightarrow ZnO + NiWO_4\left(e_{CB}^-\right) \tag{7}$$

$$NiWO_4\left(e_{CB}^-\right) + O_2 \rightarrow NiWO_4 + O_2^{\bullet-} \tag{8}$$

$$ZnO\left(h_{VB}^+\right) + MB \rightarrow CO_2 + H_2O + \text{Inorganic species} \tag{9}$$

where e_{CB}^- is the electron in the conduction band and h_{VB}^+ is the hole in the valence band, respectively.
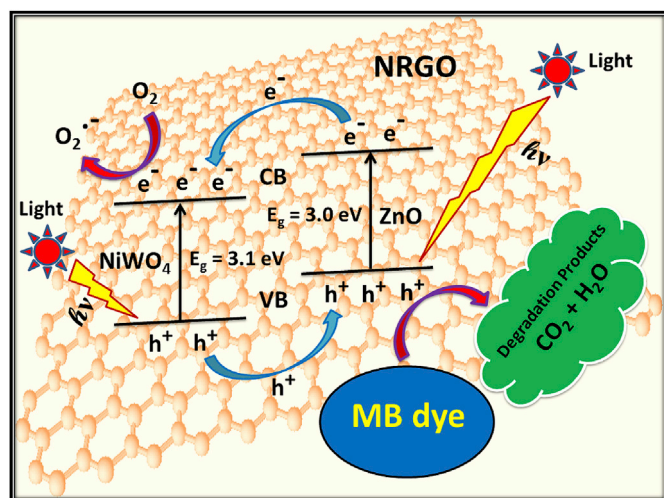
Fig. 10. Schematic diagram of photodegradation of MB over NiWO$_4$-ZnO-NRGO ternary nanocomposite under visible light irradiation.

A schematic diagram showing mechanism of photodegradation is given in Fig. 10. When ternary nanocomposite is irradiated with light, the electrons from the VB of ZnO get excited to the CB [34]. These electrons migrate to the CB of NiWO$_4$ and from there, the electrons get transferred through NRGO matrix towards reaction site. This reduces the

recombination rate of electron and holes. Then the electron combines with oxygen to form superoxide radical anion. The holes formed in the process degrade MB into products such as CO_2, H_2O and harmless species.

3.10. Reduction studies

The catalytic activity of the as-synthesized nanocomposites was evaluated by the reduction of 4-NP using NaBH$_4$ in an aqueous solution. Blank test was carried out in the absence of catalyst which showed negligible reduction of 4-NP. Addition of ternary nanocomposites into the 4-NP solution decreased the intensity of absorption peak of 4-NP found at 400 nm immediately and a new absorption peak corresponding to 4-AP at 300 nm was obtained (Fig. 11A). The catalytic reduction of 4-NP to 4-AP was completed in 80 s. This is better compared to the previously reported literature where in the conversion took 100 s [10]. For comparison, the catalytic activity of the individual components of the nanocomposite materials was analyzed and they showed lower catalytic activity than NiWO$_4$-ZnO-NRGO nanocomposites. The reaction kinetics was studied as in the case of photodegradation of MB dye (Fig. 11B–D). NiWO$_4$-ZnO-NRGO nanocomposite showed maximum rate constant 1.78 times higher than NiWO$_4$-NRGO, 2.15 times higher than ZnO-NRGO, 2.81 times than that of ZnO, 2.96 times that of NiWO$_4$ and 3.23 times that of NRGO. Further the stability and reusability of the NiWO$_4$-ZnO-NRGO ternary nanocomposites was analyzed [24]. The catalyst was recovered and further used. The reused catalyst exhibited excellent catalytic activity even after 10 successive cycles, with nearly 100%
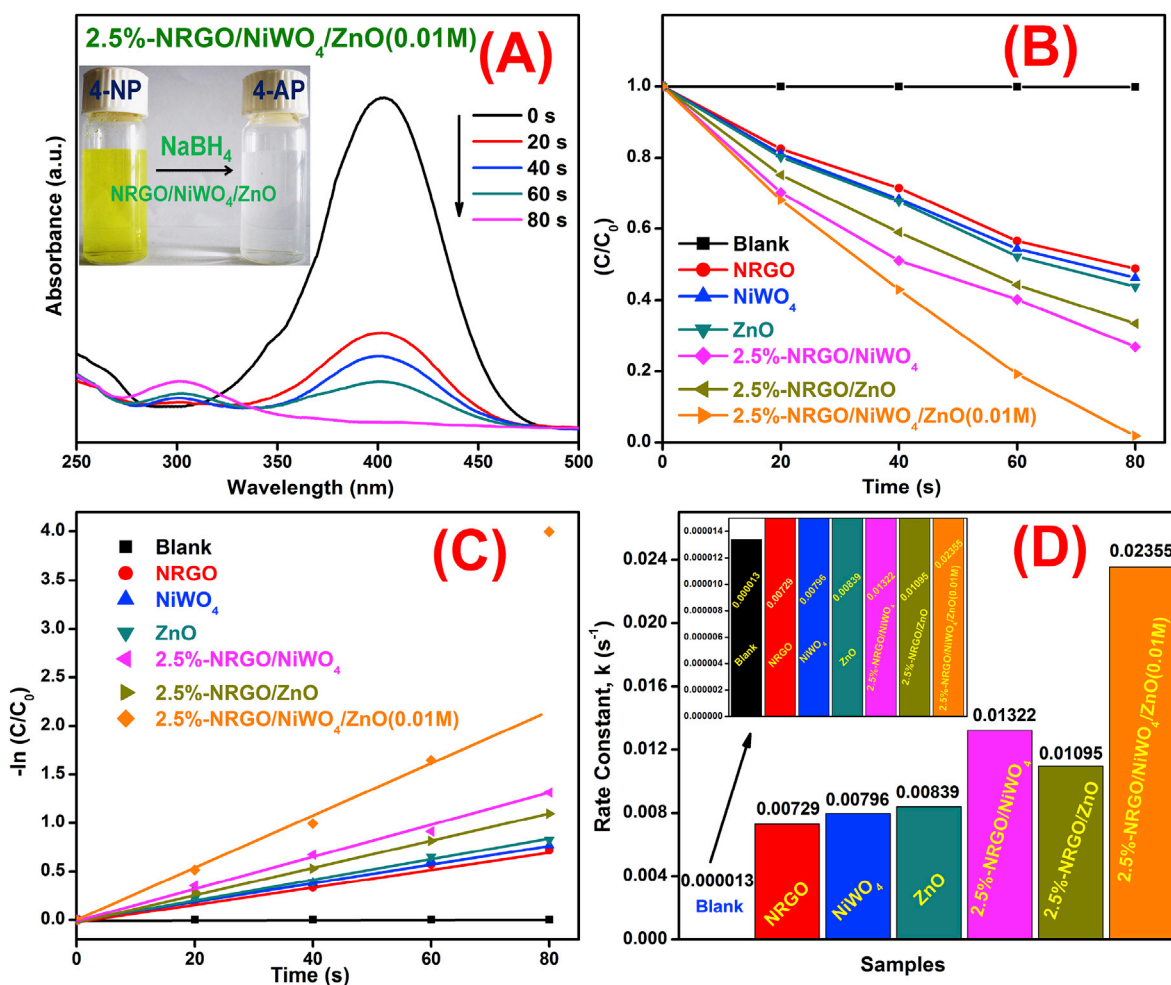

Fig. 11. (A) UV–Vis absorption spectra for the reduction of p-NP to p-AP by NaBH$_4$ in the presence of NRGO/NiWO$_4$/ZnO nanocomposite; (B) relative concentration plot of p-NP to p-AP; (C) kinetics plots and (D) rate constants of conversion of p-NP to p-AP using different catalysts.

conversion within a time period of 108 s (Fig. S6).

4. Conclusions

In this article we report successful microwave synthesis of $NiWO_4$-ZnO-NRGO ternary nanocomposites. The phase structure, elemental composition, surface morphology and optical properties of the as-synthesized nanocomposites were studied by various techniques. The visible light photocatalytic activities were studied in degradation of MB dye. Optimized concentration of efficient catalysts was found to be $NiWO_4$ – 0.01 M ZnO – 2.5% NRGO. The photodegradation efficiency of $NiWO_4$ – 0.01 M ZnO – 2.5% NRGO was approximately 9 times higher than $NiWO_4$ and it showed high stability even after 5 cycles. The formation of the band edge position followed the type II alignment and the trapping experiment suggested the photogenerated holes were the active species involved in the photocatalytic reactions. On the basis of the experimental results, the possible photodegradation mechanism was proposed. The composite also showed excellent catalytic activity in the reduction of 4-NP to 4-AP in the presence of $NaBH_4$. The reaction completed in 80 s. These results suggest that the novel ternary composite reported in the present work is a potential candidate for environmental remediation in the future and can be used for a variety of applications.

Acknowledgments

Appendix A. Supplementary data

Supplementary data related to this article can be found at http://dx.doi.org/10.1016/j.jpcs.2017.05.023.

References

[1] D. Chen, H. Zhu, S. Yang, N. Li, Q. Xu, H. Li, J. He, J. Lu, Micro-nanocomposites in environmental management, Adv. Mater. 28 (2016) 10443–10458.

[2] M. Ahmad, E. Ahmed, Z.L. Hong, J.F. Xu, N.R. Khalid, A. Elhissi, W. Ahmed, A facile one-step approach to synthesizing ZnO/graphene composites for enhanced degradation of methylene blue under visible light, Appl. Surf. Sci. 274 (2013) 273–281.

[3] A.S. Bhatt, D.K. Bhat, Influence of nanoscale NiO on magnetic and electrochemical behavior of PVDF based polymer nanocomposites, Polym. Bull. 68 (2012) 253–261.

[4] M. Selvakumar, D.K. Bhat, Microwave-assisted synthesis of TiO2 nano particles and its electrochemical properties with activated carbon, Appl. Surf. Sci. 263 (2012) 236–241.

[5] A.S. Bhatt, D.K. Bhat, M.S. Santosh, Crystallinity, conductivity and magnetic properties of PVDF-Fe3O4 composite films, J. Appl. Polym. Sci. 119 (2011) 968–972.

[6] A.S. Bhatt, D.K. Bhat, Crystallinity, magnetic and electrochemical studies of PVDF/Co3O4 polymer electrolyte, Mater. Sci. Engg. B 177 (2012) 127–131.

[7] M. Pirhashemi, A.H. Yangjeh, Ultrasonic-assisted preparation of plasmonic ZnO/Ag/Ag2WO4 nanocomposites with high visible light photocatalytic performance for degradation of organic pollutants, J. Colloid Interface Sci. 491 (2017) 216–229.

[8] T. Hisatomi, J. Kubota, K. Domen, Recent advances in semiconductors for photocatalytic and photoelectrochemical water splitting, Chem. Soc. Rev. 43 (2014) 7520–7535.

[9] M.M.J. Sadiq, D.K. Bhat, A facile microwave approach to synthesize RGO-BaWO4 composites for high performance visible light induced photocatalytic degradation of dyes, AIMS Mater. Sci. 4 (2017) 487–502.

[10] M.M.J. Sadiq, U.S. Shenoy, D.K. Bhat, High performance bifunctional catalytic activity of novel zinc tungstate – reduced graphene oxide nanocomposite, Adv. Sci. Eng. Med. 9 (2017) 115–121.

[11] B. Subramanya, D.K. Bhat, S.U. Shenoy, Y. Ullal, A.C. Hegde, Novel Fe-Ni-Graphene composite electrode for hydrogen production, Int. J. Hydrogen Energy 40 (2015) 10453–10462.

[12] B. Subramanya, Y. Ullal, S.U. Shenoy, D.K. Bhat, A.C. Hegde, Novel Co-Ni-Graphene composite electrodes for hydrogen production, RSC Adv. 5 (2015) 47398–47407.

[13] S. Banerjee, S.C. Pillai, P. Falaras, K.E. Oshea, J.A. Byrne, D.D. Dionysiou, New insights into the mechanism of visible light photocatalysis, J. Phys. Chem. Lett. 5 (2014) 2543–2554.

[14] M. Farhadian, P. Sangpour, G. Hosseinzadeh, Preparation and photocatalytic activity of WO3-MWCNT nanocomposite for degradation of naphthalene under visible light irradiation, RSC Adv. 6 (2016) 39063–39073.

[15] Z. Jafari, N. Mokhtarian, G. Hosseinzadeh, M. Farhadian, A. Faghihi, F. Shojaie, Ag/TiO2/freeze-dried graphene nanocomposite as a high performance photocatalyst under visible light irradiation, J. Energy Chem. 25 (2016) 393–402.

[16] A.H. Keihan, R. Hosseinzadeh, M. Farhadian, H. Kooshki, G. Hosseinzadeh, Solvothermal preparation of Ag nanoparticle and graphene co-loaded TiO2 for Photocatalytic degradation of paraoxon pesticide under visible light irradiation, RSC Adv. 6 (2016) 83673–83687.

[17] Q. Xiang, D. Lang, T. Shen, F. Liu, Graphene-modified nanosized Ag3PO4 photocatalysts for enhanced visible-light photocatalytic activity and stability, Appl. Cat. B Environ. 162 (2015) 196–203.

[18] K. Dai, X. Zhang, K. Fan, T. Peng, B. Wei, Hydrothermal synthesis of single-walled carbon nanotube-TiO2 hybrid and its photocatalytic activity, Appl. Surf. Sci. 270 (2013) 238–244.

[19] H. Zhang, X. Fan, X. Quan, S. Chen, H. Yu, Graphene sheets grafted Ag@AgCl hybrid with enhanced plasmonic photocatalytic activity under visible light, Environ. Sci. Technol. 45 (2011) 5731–5736.

[20] X. Li, H. Wang, J.T. Robinson, H. Sanchez, G. Diankov, H. Dai, Simultaneous nitrogen doping and reduction of graphene oxide, J. Am. Chem. Soc. 131 (2009) 15939–15944.

[21] M.M.J. Sadiq, U.S. Shenoy, D.K. Bhat, Enhanced photocatalytic performance of N-doped RGO-FeWO4/Fe3O4 ternary nanocomposite in environmental applications, Mat. Today. Chem. 4 (2017) 133–141.

[22] M.M.J. Sadiq, U.S. Shenoy, D.K. Bhat, Novel RGO–ZnWO4–Fe3O4 nanocomposite as high performance visible light photocatalyst, RSC Adv. 6 (2016) 61821–61829.

[23] H. Chang, H. Wu, Graphene-based nanocomposites: preparation, functionalization and energy and environmental applications, Energy Environ. Sci. 6 (2013) 3483–3507.

[24] M.M.J. Sadiq, D.K. Bhat, Novel RGO–ZnWO4–Fe3O4 nanocomposite as an efficient catalyst for rapid reduction of 4-nitrophenol to 4-aminophenol, Ind. Eng. Chem. Res. 55 (2016) 7267–7272.

[25] M.M.J. Sadiq, D.K. Bhat, Novel ZnWO4/RGO nanocomposite as high performance photocatalyst, AIMS Mater. Sci. 4 (2017) 158–171.

[26] D.K. Bhat, Facile synthesis of ZnO nanorods by microwave irradiation of zinc-hydrazine hydrate complex, Nanoscale Res. Lett. 3 (2008) 31–35.

[27] B. Subramanya, D.K. Bhat, Novel eco-friendly synthesis of graphene directly from graphite using 2,2,6,6-tetramethylpiperidine 1-oxyl and study of its electrochemical properties, J. Power Sources 275 (2015) 90–98.

[28] B. Subramanya, D.K. Bhat, Novel one-pot green synthesis of graphene in aqueous medium under microwave irradiation using regenerative catalyst and study of its electrochemical properties, New J. Chem. 39 (2014) 420–430.

[29] G. Chen, H. Guan, C. Dong, X. Xiao, Y. Wang, Effect of calcination temperatures on the electrochemical performances of nickel oxide/reduction graphene oxide (NiO/RGO) composites synthesized by hydrothermal method, J. Phys. Chem. Solids 98 (2016) 209–219.

[30] Y. Ma, Y. Guo, H. Jiang, D. Qu, J. Liu, W. Kang, Y. Yi, W. Zhang, J. Shi, Z. Han, Preparation of network-like ZnO-FeWO4 mesoporous heterojunctions with tunable band gaps and their enhanced visible light photocatalytic performance, New J. Chem. 39 (2015) 5612–5620.

[31] L. Wang, J. Ding, Y. Chai, Q. Liu, J. Ren, X. Liu, W.L. Dai, CeO2 nanorods/g-C3N4/N-rGO composite: enhanced visible-light driven photocatalytic performance and the role of N-rGO as electronic transfer media, Dalton Trans. 44 (2015) 11223–11234.

[32] A. Meng, J. Shao, X. Fan, J. Wang, Z. Li, Rapid synthesis of a flower-like ZnO/rGO/Ag micro/nano-composite with enhanced photocatalytic performance by a one-step microwave method, RSC Adv. 4 (2014) 60300–60305.

[33] Y. Cui, H. Li, W. Hong, S. Fan, L. Zhu, The effect of carbon content on the structure and photocatalytic activity of nano-Bi2WO6 powder, Powder Technol. 247 (2013) 151–160.

[34] J. Xu, Y. Cui, Y. Han, M. Hao, X. Zhang, ZnO-graphene composites with high photocatalytic activities under visible light, RSC Adv. 6 (2016) 96778–96784.